

Aerial Sensing and Characterization of Three-Dimensional RF Fields

Ervin Teng
ervin.teng@sv.cmu.edu

Frank Mokaya
frank.mokaya@sv.cmu.edu

Joao Diogo Falcao
joaodf@cmu.edu

Pei Zhang
peizhang@cmu.edu

Carlos Ruiz Dominguez
carlosrd@cmu.edu

Bob Iannucci
bob@sv.cmu.edu

Carnegie Mellon University
Building 23, NASA Ames Research Park
Moffett Field, CA 94035

ABSTRACT

Beyond military, hobby and recreational use, Unmanned Aerial Vehicles (UAVs) and the potential they represent are being considered seriously for a variety of commercial applications. While a number of regulatory, safety and privacy issues remain to be resolved, several interesting technical challenges have presented themselves. In particular, we predict a trend in which commercial UAVs will move from point-to-point radio systems for command, control and telemetry to using commercial cellular networks, primarily because such networks offer broad coverage. Commercial services have already emerged to provide cloud-based UAV control via cellular networks. But a significant problem remains – these networks were planned, designed and engineered for ground-based terminal devices. The skies are poorly characterized in terms of cellular coverage, leading to risks associated with planning and flying missions into the radio unknown.

Prompted by the UAV opportunity, an examination of cellular network planning – from an RF perspective – reveals that the models used are likewise biased by the ground-based assumption. In this research, we focus on the challenges of characterizing cellular and other multi-node networks in three dimensions, leading to a re-consideration of how measurement and modeling can be beneficially combined. This work suggests potential improvements in the speed and accuracy of multi-node radio network planning and deployment with application to UAVs, hastily-formed (*e.g.*, emergency) networks, and general network design and optimization.

Categories and Subject Descriptors

C.2.1 [Computer-Communication Networks]: Network Architecture and Design—*Wireless communication*; I.2.9 [Artificial Intelligence]: Robotics—*Autonomous Vehicles*; C.4 [Performance of Systems]: [Modeling techniques]

Permission to make digital or hard copies of all or part of this work for personal or classroom use is granted without fee provided that copies are not made or distributed for profit or commercial advantage and that copies bear this notice and the full citation on the first page. To copy otherwise, to republish, to post on servers or to redistribute to lists, requires prior specific permission and/or a fee.

Copyright 20XX ACM X-XXXXX-XX-X/XX/XX ...\$15.00.

Keywords

Wireless Propagation, Unmanned Aerial Systems, Coverage Mapping

1. INTRODUCTION

The proliferation of low-cost GPSs, inertial sensors, and processing, due in no small part to the growing popularity of smartphones, has significantly lowered the price of navigation-capable unmanned aerial vehicles (UAVs). Once only found in the realm of high-budget military applications, small UAVs are now available for a variety of civil uses, from law enforcement to amateur photography. Typical civilian UAVs rely on a single point-to-point link between the aircraft and an operator on the ground for telemetry as well as command and control.

We can easily envision applications that would require connectivity beyond a single ground-based transmitter, such as goods delivery or wide-area surveillance and monitoring. Unable to rely on the exceedingly expensive and limited satellite uplinks typically used in military systems, civilian UAVs must rely on terrestrial wide-area networks (WAN) for beyond-LOS connectivity. A high-bandwidth connection, especially for processing-constrained UAVs, could also boost navigation with the implementation of cloud-based data processing [10, 13].

Cellular networks can be a solution for communication with UAVs over populated areas; wide area coverage, low cost of integration, packet-switched data capability, and sub-100ms latencies for LTE [8] make telemetry and command-and-control of UAVs, even with in-flight transmission of video or images, possible. Indeed, commercial products that use cellular networks for telemetry exist [1]. However, today's cellular networks are first and foremost designed for users on the ground, and the above-ground coverage is not well characterized and thus cannot be assumed as reliable [5]. Furthermore, the primary tools used to plan and evaluate such networks, namely, RF propagation models, often do not apply in scenarios where the antenna is lower in altitude than the receiving device [6].

In this paper, we seek to build a better understanding of RF propagation in three dimensions, especially in the context of rapidly deployable cellular networks. To do so, we present:

- A system that takes aerial measurements *in situ* via

UAV

- A method to quickly and simply visualize the measured RF field as the data is collected
- A comparison of the data against an existing propagation model designed for on-the-ground applications, and further trend analysis

The rest of this paper is structured as follows. In Section 3, we detail the system we designed to take these measurements. In Section 4, we detail the experimental scenario. In Section 5, we present an analysis of the collected data. Finally, in Section 6, we present our conclusions and outline possibilities for future work.

2. BACKGROUND

In order to predict wireless coverage before deployment, a network operator can use a propagation model. Numerous RF models for “tall” transmitters and receivers on the ground (*i.e.*, the cellular case) have been created from collected data [11], extended [7], compared [9, 2], and optimized [3]. They are widely used in the planning and optimization of cellular and other wireless networks [6]. They can roughly be divided into two categories: statistical or empirical, and deterministic. Empirical models, such as the commonly used Okumura-Hata model [7], are created based on real measurements in various scenarios, and are typically computationally light but less accurate. Deterministic models can achieve very high accuracies using techniques such as ray-tracing, but rely on detailed models of the environment and require significant computation. The COST231 project assembled and improved a collection of these models for use by wireless deployments [4].

2.1 COST-231 Walfisch-Ikegami Model

Here, we examine in more detail one of these models, the COST-231 version of the Walfisch-Ikegami model [4]. It is, unlike the Okumura-Hata model, a semi-deterministic model, in that it takes into account some aspects of the environment but still considers them in aggregate (*e.g.*, average building height rather than individual). It is chosen here as a starting point because it both applicable to small cells (cellular transmitters) below and above the building height, and for relatively short distances $> 20\text{m}$. The model takes into account:

- Frequency f in MHz
- Ground distance from TX to RX d in km
- Transmitter height h_{TX}
- Receiver height h_{RX}
- Height of buildings h_{roof}
- Width of roads w_{road}
- Building separation b_{sep}
- Angle between roads and direct radio path ϕ

For non-line-of-sight (NLOS) between the transmitter and receiver, the path loss is defined as follows:

$$L_{NLOS} = L_{fs} + L_{rts} + L_{msd} \quad (1)$$

where L_{fs} is free-space loss described in Equation 2, and L_{rts} , L_{msd} are estimated rooftop-to-street diffraction/scatter and multiscreen diffraction loss, respectively. L_{fs} is the minimum loss; if $L_{rts} + L_{msd} < 0$, $L_{NLOS} = L_{fs}$.

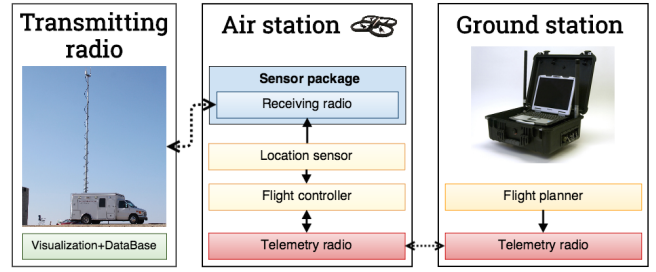


Figure 1: System architecture

$$L_{fs} = 32.4 + 20\log(d) + 20\log(f) \quad (2)$$

The loss estimates described in Equations 3 and 4 hold for situations where the transmitter is above the heights of the buildings, and ϕ is large (55 to 90 degrees).

$$L_{rts} = -16.9 - 10\log(w_{road}) + 10\log(f) + 20\log(h_{roof} - h_{RX}) + (4 - 0.114(\phi - 55)) \quad (3)$$

$$L_{msd} = k_a + k_b + k_c \log(d) + k_d \log(f) - 9\log(b)$$

$$k_a = -18\log(1 + h_{TX} - h_{roof})$$

$$k_b = 54$$

$$k_c = 18$$

$$k_d = -4 + 0.7\left(\frac{f}{925} - 1\right) \quad (4)$$

Given Equation 3, we see that it is expected in the model that the RX is *below* the heights of the buildings. There is no provision for having a TX and RX that are above the heights of the buildings, as is often the case when the RX is a UAV. We will again explore this issue in Section 5, where we will compare collected aerial data to this model.

2.2 Models for Aerial Vehicles

Aerial RF surveys of existing cellular networks at altitude have in the past been conducted from manned aircraft [12], with the intent of placing cellular calls while in flight. More recently, there has been work in characterizing the path loss [16] and performance [17] of WiFi signals at heights relevant to sUAS systems. These authors evaluate the performance of the WiFi system at various distances and UAV orientations, as well as present a simple logarithmic (1D) model for the data. In urban environments, there has also been work to adapt the pre-existing urban propagation models to UAV applications [14], taking into account diffraction off buildings. This work focuses on the point-to-point operator case, where the UAV communicates with a single ground station at human heights below the surrounding rooftops.

3. APPROACH OVERVIEW

In order to take aerial signal strength measurements, relay the results on the ground, and visualize the data in real-time, we construct a system consisting of a ground station, an air station and the target antenna(s). A diagram of the system is shown in Figure 1.

3.1 Transmitting Radio and Data Collection

The transmitting radio is our proxy for a cellular base station. It consists of a 915MHz (ISM) serial radio based on the HopeRF chipset, capable of both transmitting and receiving data over a serial interface; this band was chosen as representative, propagation-wise, of a 900MHz cellular system, such as GSM900 and UMTS/LTE band 9. A similarly configured radio is affixed to the air station and receives packets from the transmitting antenna, measures the signal strength, and relays the signal strength back to the transmitting radio, where the data is logged in a database. We thus not only record the signal's strength from the point of view of the UAV, but also from the base station's point of view. This data can then be plotted on a map and displayed in real-time using a web application.

3.2 Ground station

The ground station is responsible for flight planning and UAV control as well as telemetry, and consists of a laptop computer and a telemetry radio. To avoid interference with the 915MHz sensing, this radio operates at 433MHz. At the ground station, the operator can specify the waypoints, as GPS coordinates on a map, the drone should fly during a mission. For this study, the missions have to be loaded in advance for the drone to cover the area, although we can imagine data-driven real-time flight planning as a superior option and future direction.

3.3 Air station

The air station is composed of a UAV and flight control system carrying a sensing package (described in the following section). The UAV itself is a quadcopter custom-built from off-the-shelf components, with enough capacity to carry a variety of sensor payloads. The flight controller is a 3D Robotics PixHawk running the open-source ArduPilot software; attached to this controller is an SBAS-capable GPS unit and 433MHz telemetry radio, allowing for drone telemetry and control separate from the radio used for sensing. The flight controller also simultaneously reports its GPS location and altitude to the sensing package.

3.4 Sensor Package

The sensor package consists of a single 915MHz ISM-band radio, paired with the TX under test. As the sensing radio receives packets from the transmitting radio, it aggregates the location and altitude from the flight controller with the received signal strength, and transmits it back to the transmitting radio. An important consideration for the receive antenna is that, being a dipole with ground plane, its gain is not uniform in the vertical plane. This means that as the quadcopter pitches and rolls, the gain towards the direction of the transmitting antenna will change significantly. Thus, a brushless gimbal, commonly used for aerial photography, is utilized to keep the receive antenna pointing towards the ground regardless of the UAV's angle of attack. Figure 2 shows the gimbal in flight.

4. EXPERIMENTS

We conducted several propagation studies at a Joint Inter-agency Field Experimentation (JIFX) event, held by the Naval Postgraduate School at Camp Roberts, CA. We conducted experiments with the same transmitter at a variety of scenarios:

- Rural urban environment
- Collapsed buildings
- Open field

For each of these scenarios we flew the UAV with different patterns: *3D lawn-mower*, spirals and manual flight around and above buildings.

The cellular signal strength is more likely to be affected by the environment in an urban scenario than in an open field. Therefore this paper focuses on that scenario.

Our transmitter-under-test, in this case, is a mobile communications van, shown in Figure [1], equipped with a self-contained, rapidly deployable cellular network operating in the GSM900 band. For this experiment, we replaced the GSM base station with our 915MHz transmitting radio. The van also contains the servers and monitor necessary to record incoming data and perform visualizations. Atop the van's 45-foot pneumatic mast is an L-com HGV-906U, a 6dBi omni-directional antenna with a vertical beam width of 30 degrees. All in all, with the mast fully extended the antenna is located 13.9 meters above ground level. The spot at which the van was parked was 257m above sea level (ASL).

Although the mast fully extends beyond the altitude of some of the buildings, it is still relevant to map the signal strength over those buildings to observe any reflection or



Figure 2: A gimbal keeps the antenna perpendicular to the ground regardless of the drone's angle of attack

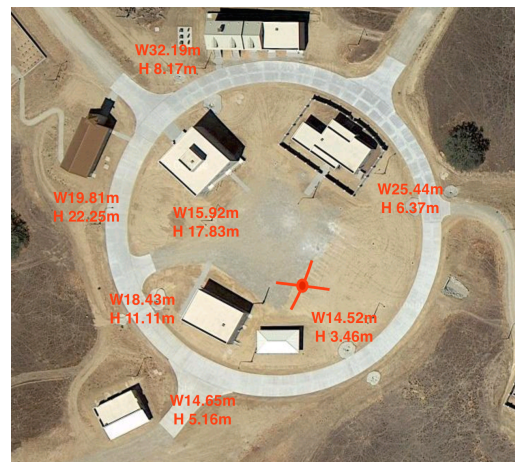


Figure 3: Location of the ground station. Rural Urban Environment at Camp Roberts, Paso Robles

refraction that might occur. Our flights include data gathered from above and below the mast altitude, as well as over the buildings and in between them. Figure 3 shows the surrounding buildings with their approximate corresponding dimensions and the location of our transmitting antenna.

For this experiment, we transmit our test packets from the radio-under-test at 20dBm.

5. RESULTS AND ANALYSIS

In this section, we visualize and analyze the data collected in the urban environment experiment described in Section 4.

5.1 RF Mapping and Interpolation

The first application of our captured data is to create a three-dimensional map of signal strength in the target area. If done quickly or even as the UAV completes its mission, this gives the network planner an idea of how the transmitter is performing and where additional measurements are needed, guiding the following missions.

In order to deal with the intrinsically noisy data from our sensor, we first create a grid of points in the area of interest, at the desired resolution. At each point on the grid, we bin the raw data that falls within a sphere around that point, and assign the averaged value of the RSSIs of the binned datum to the point. This results in a decimated regular grid of points. To fill the rest of the grid, we use a natural neighbor interpolation algorithm [15], chosen for its exact interpolation of known points and its smoothness between these points. Since signal strength in dB falls logarithmically with distance, and natural neighbor is fundamentally linear, we linearize and scale the data with Equation 5 before applying interpolation, and reverse the operation on the interpolated data.

$$P_{linear} = 10^{-P_{dBm}/2000} \quad (5)$$

Figure 4 shows raw data gathered within a 500 meter radius of our transmitting antenna, with the color representing the received signal strength in dBm, as shown by the legend. We subdivide this 1500x1300x150m area into a 100x100x50 grid, and decimate using a binning radius of 20m, resulting in Figure 5. We then apply a natural neighbor interpolation algorithm to the decimated data.

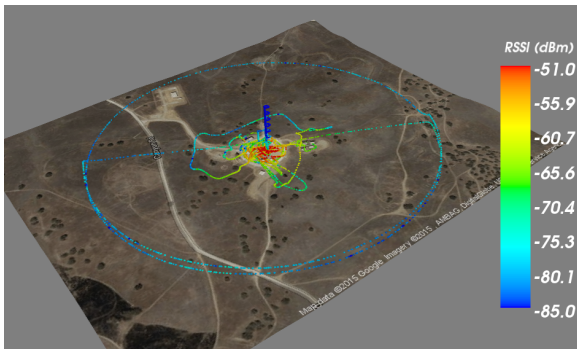


Figure 4: Raw flight data.

Figure 6 shows a slice at 275m ASL. At this altitude, we strongly see the effect of the transmitting antenna and the rapid falloff of signal strength.

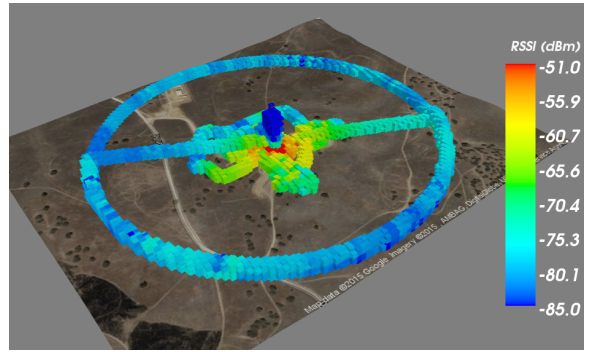


Figure 5: Data binned into 20m radius spheres on a regular grid.

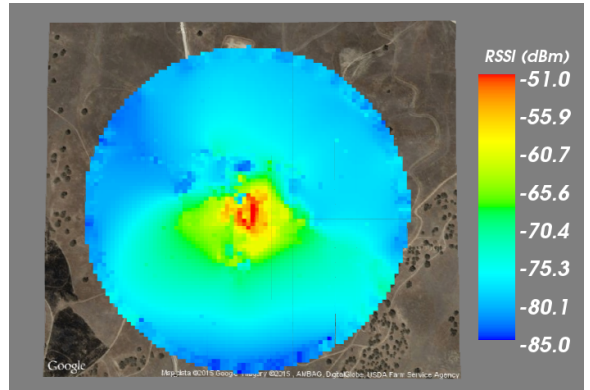


Figure 6: Z-axis slice at 275m ASL.

Figure 7 shows a vertical slice. Note the narrow beam width of the transmitting antenna, and the rapid falloff of signal strength above the antenna.

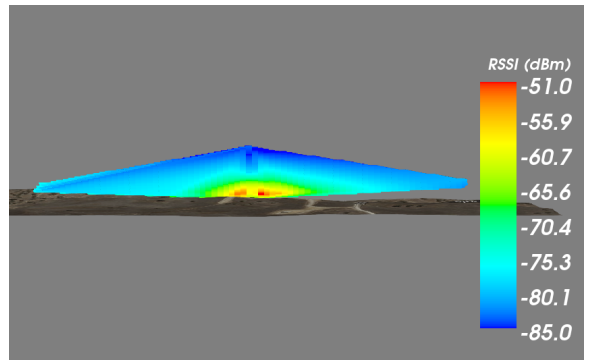


Figure 7: Vertical slice

We now repeat the process with only the data in the center 50m circle. We decrease the binning radius to 2m, and increase the resolution (over the same area) of the grid to 300x300x50. In Figure 8, we see a top-down slice of the data, revealing more nuanced features such as the radio shadow caused by the buildings.

We recognize that the fidelity of these RF maps is directly related to the density of sampled points. Without decimation, interpolation can generate artifacts from the noisy

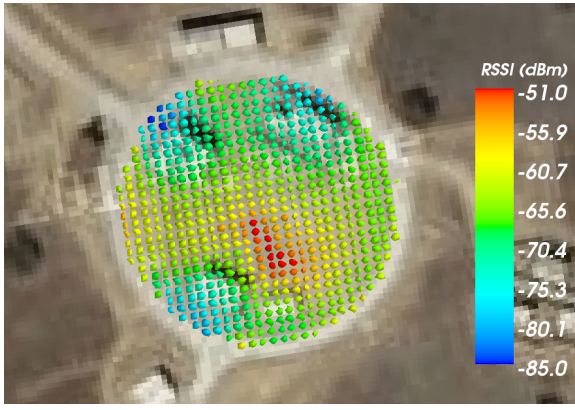


Figure 8: Z-axis slice at 265m

Table 1: Parameters for COST231-WI Model

Parameter	Value
h_{TX}	13.9m
h_{roof}	9.76m
w_{road}	16.94m
b_{sep}	16.43m
ϕ	90°

data. Decimation, however, reduces resolution.

5.2 Comparison with Propagation Models

We now compare our aerial data with the COST231-WI model presented in Section 2.1, with one caveat. As it would be invalid with RX heights above the roof heights, we omit the second-to-last term of Equation 3, with the assumption that it becomes incredibly small with increasing RX height. We use the parameters in Table 1, estimated from the geometries of the buildings surrounding the transmitters.

In addition to the path loss given by the model, we also take into account the radiation pattern of our transmitting antenna and 5 dB of cable and connector loss at both the transmitter and receiver. Figure 9 shows the binned data, plotted vs. distance from the transmitter, and the predicted RSSI values based on the COST-231-WI model at the same points. We remove the values before 20m, as the model is not valid for these points.

We note that the model produces an upper bound on the signal strength, and the data respects that. Also, the slope (path loss exponent) is fairly similar. We also note that data shows a wide variance at any given distance.

5.2.1 Regression Analysis

In order to better understand the trends in our data, we apply a least-squared regression to the decimated data. In accordance with the free-space propagation Equation 2, we assume the path loss follows the general trend given by Equation 6.

$$L_{prop} = L_{d0} + \alpha \log\left(\frac{d}{d0}\right) \quad (6)$$

where L_{d0} is the propagation loss at a reference distance

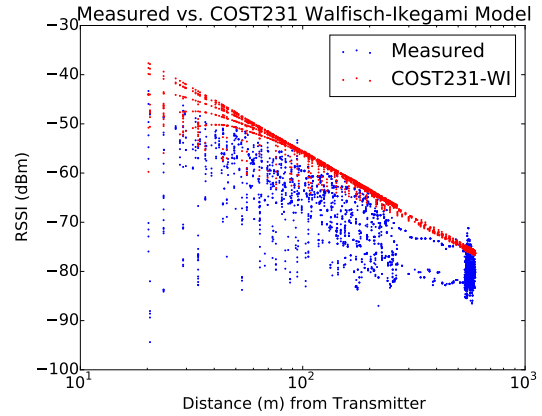


Figure 9: Comparison of binned data vs. predicted COST-231-WI measurements

$d0$, and α is the path loss exponent. We choose the reference distance to be 20m. In order to compute path loss, we subtract the RSSI in dBm from the expected transmit power at the antenna, given its gain pattern. Figure 10 shows a comparison of the decimated data with the least-squares fit of Equation 6.

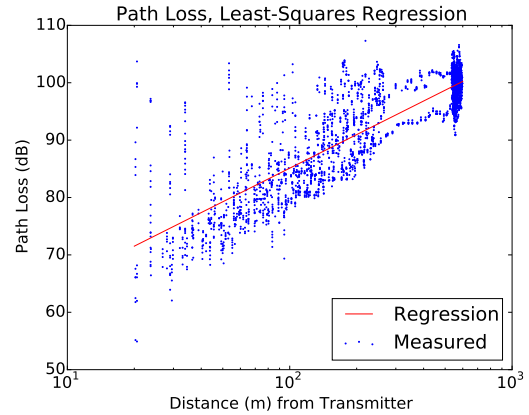


Figure 10: Path Loss vs. Distance, Least-squared fit

We note that $\alpha = 19.4$ and the path loss L_{d0} at 20m is 71.5 dB. This compares favorably with the $\alpha = 18$ prescribed by the COST-231 Walfisch-Ikegami model in Equation 4, and the $\alpha = 20$ described in the free-space propagation loss equation 2. Note that there are other effects that are insufficiently described by a distance-dependent fit. For instance, Figure 11 shows the path loss, after accounting for antenna gain pattern, at two altitude slices.

We see that there is some altitude dependency on path loss that cannot be accounted for in our current analysis. Further data collection is required to accurately model this effect.

6. CONCLUSION AND FUTURE WORK

In this paper, we collect and examine RF field strength data above ground, with the intention of better understanding field propagation in the context of using terrestrial cel-

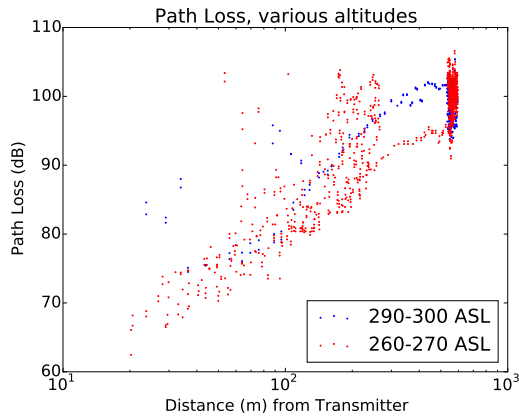


Figure 11: Path Loss vs. Distance, Least-squared fit

lular networks to communicate with small UAVs in the air. To do this, we develop a system for autonomously collecting, storing, and visualizing this data, consisting of both a UAV aerial station and a ground station. We analyze received signal strength data collected from a transmitter emulating a rapidly deployed cellular base station in an urban environment. We reveal that while the general trends match existing terrestrial propagation models, there is still work to be done to more accurately represent the space.

The current data set is too sparse, however, to definitively create a propagation model that could be applied to similar situations. Our future work, thus, will involve collecting similar sets of data at finer altitude scales in order to establish an altitude dependence on the data. In addition, we plan to examine this data in the context of the exact geometries and positioning of the buildings and terrain, their intrusions into the Fresnel zone of our transmissions, and the corresponding diffraction and reflection effects.

7. ACKNOWLEDGMENTS

We would like to thank the Naval Postgraduate School for their sponsorship of the Joint Interagency Field Experiments (JIFX) that provided us with the opportunity to make realistic *in situ* measurements. We also thank CMU's College of Engineering for the research equipment grant supporting creation of the mobile communications van critical to these studies. Additionally, we want to give our thanks to Nokia for sponsoring our travel to Camp Roberts to attend the JIFX event. This work was partially funded by the NSF (grant CNS1135874).

8. REFERENCES

- [1] Dronedeploy. <http://www.dronedeploy.com>.
- [2] P. Begovic, N. Behlilovic, and E. Avdic. Applicability evaluation of Okumura, Ericsson 9999 and winner propagation models for coverage planning in 3.5 GHZ WiMAX systems, 2012.
- [3] L. Benedičič, M. Pesko, P. Korošec, and T. Javornik. A Metaheuristic Approach for Propagation-Model Tuning in LTE Networks. *Informatika*, 38:135–143, 2014.
- [4] D. Cichon and T. Kurner. Propagation prediction models. In *COST 231 Final Report*, pages 116–208.

- 1995.
- [5] K. Daniel and C. Wietfeld. Using Public Network Infrastructures for UAV Remote Sensing in Civilian Security Operations. *Homeland Security Affairs*, 3, 2011.
- [6] ETSI. GSM 03.30 version 5.0.0, 1996.
- [7] M. Hata. Empirical Formula for Propagation Loss in Land Mobile Radio Services. *IEEE Transactions on Vehicular Technology*, 29:317–325, 1980.
- [8] J. Huang, F. Qian, A. Gerber, and Z. Mao. A Close Examination of Performance and Power Characteristics of 4G LTE Networks. In *Proceedings of the 10th international conference on Mobile systems, applications, and services*, pages 225–238, 2012.
- [9] J. Milanović, S. Rimac-drlje, and I. Majerski. Radio wave propagation mechanisms and empirical models for fixed wireless access systems. *Technical Gazette*, 733(2):43–52, 2010.
- [10] T. Mori and S. Scherer. First results in detecting and avoiding frontal obstacles from a monocular camera for micro unmanned aerial vehicles. In *2013 IEEE International Conference on Robotics and Automation*, pages 1750–1757. IEEE, May 2013.
- [11] Y. Okumura, E. Ohmori, T. Kawano, and K. Fukuda. Field strength and its variability in VHF and UHF land-mobile radio service. *Review of the Electrical Communication Laboratory*, 16:825–873, 1968.
- [12] J. A. Romo, G. Aranguren, J. Bilbao, I. n. Odriozola, J. Gómez, and L. Serrano. GSM / GPRS Signal Strength Measurements in aircraft flights under 3,000 meters of altitude. *WSEAS Transactions on Signal Processing*, 5(6):219–228, 2009.
- [13] S. Ross, N. Melik-Barkhudarov, K. S. Shankar, A. Wendel, D. Dey, J. A. Bagnell, and M. Hebert. Learning monocular reactive UAV control in cluttered natural environments. In *2013 IEEE International Conference on Robotics and Automation*, pages 1765–1772. IEEE, May 2013.
- [14] M. Simunek, P. Pechac, and F. P. Fontan. Excess loss model for low elevation links in urban areas for UAVs. *Radioengineering*, 20(3):561–560, 2011.
- [15] N. Sukumar. A note on natural neighbor interpolation and the natural element method (NEM). 1997.
- [16] E. Yanmaz, R. Kuschnig, and C. Bettstetter. Channel measurements over 802.11a-based UAV-to-ground links. In *2011 IEEE GLOBECOM Workshops, GC Wkshps 2011*, pages 1280–1284, 2011.
- [17] E. Yanmaz, R. Kuschnig, and C. Bettstetter. Achieving air-ground communications in 802.11 networks with three-dimensional aerial mobility. In *Proceedings - IEEE INFOCOM*, pages 120–124, 2013.